

HIV-1 Nef Inhibits Ruffles, Induces Filopodia, and Modulates Migration of Infected Lymphocytes[∇]

Cinzia Nobile,^{1,6†} Dominika Rudnicka,^{1†} Milena Hasan,² Nathalie Aulner,³ Françoise Porrot,¹ Christophe Machu,³ Olivier Renaud,⁴ Marie-Christine Prévost,⁵ Claire HIVroz,⁶ Olivier Schwartz,^{1*†} and Nathalie Sol-Foulon^{1*†}

Virus and Immunity Unit, Department of Virology, Institut Pasteur, URA CNRS 3015, 28 rue du Dr. Roux, 75724 Paris Cedex 15, France¹; Centre d'Immunologie Humaine (CIH), Institut Pasteur, Paris, France²; Imagopole, Institut Pasteur, Paris, France³; Institut Curie, Imagerie Cellulaire et Tissulaire—UMR 3215 (pict-IBiSA), 26 rue d'Ulm, 75248 Paris Cedex 05, France⁴; Electron Microscopy Core Facility, Institut Pasteur, Paris, France⁵; and Institut Curie, Centre de Recherche, Inserm Unité 932, Paris, France⁶

Received 22 October 2009/Accepted 3 December 2009

The HIV-1 Nef protein is a pathogenic factor modulating the behavior of infected cells. Nef induces actin cytoskeleton changes and impairs cell migration toward chemokines. We further characterized the morphology, cytoskeleton dynamics, and motility of HIV-1-infected lymphocytes. By using scanning electron microscopy, confocal immunofluorescence microscopy, and ImageStream technology, which combines flow cytometry and automated imaging, we report that HIV-1 induces a characteristic remodeling of the actin cytoskeleton. In infected lymphocytes, ruffle formation is inhibited, whereas long, thin filopodium-like protrusions are induced. Cells infected with HIV with *nef* deleted display a normal phenotype, and Nef expression alone, in the absence of other viral proteins, induces morphological changes. We also used an innovative imaging system to immobilize and visualize living individual cells in suspension. When combined with confocal “axial tomography,” this technique greatly enhances three-dimensional optical resolution. With this technique, we confirmed the induction of long filopodium-like structures in uninfected Nef-expressing lymphocytes. The cytoskeleton reorganization induced by Nef is associated with an important impairment of cell movements. The adhesion and spreading of infected cells to fibronectin, their spontaneous motility, and their migration toward chemokines (CXCL12, CCL3, and CCL19) were all significantly decreased. Therefore, Nef induces complex effects on the lymphocyte actin cytoskeleton and cellular morphology, which likely impacts the capacity of infected cells to circulate and to encounter and communicate with bystander cells.

Human immunodeficiency virus type 1 (HIV-1) mostly replicates in T-cell areas of secondary lymphoid organs (SLOs) and induces pathological changes in their architecture. Such changes are likely due to a combination of events, including destruction of T cells, chronic immune activation, and alteration of T-cell motility toward and inside the SLOs (27, 37, 50, 53). Indeed, to fulfill their immune surveillance role, T cells continuously circulate in and out of blood, lymph nodes (LNs), and tissues (60).

Lymphocyte recruitment from the bloodstream into LNs depends on three distinct processes, i.e., attachment to high endothelial venules (HEVs), extravasation, and cell migration (10, 60). Adhesion to the endothelium and extracellular matrix (ECM) is a crucial step, regulated in part by $\beta 1$ integrins, $\alpha 4\beta 1$ (VLA-4) and $\alpha 5\beta 1$, that bind VCAM-1 and/or fibronectin (56). Chemokines and their G α i-protein-coupled receptors are key regulators of lymphocyte trafficking (32). For instance, CCL19

and CCL21 are constitutively produced by HEVs and by fibroblastic reticular cells of T-cell areas of LNs (21, 28, 29). These two chemokines share the receptor CCR7, expressed by naïve T cells and a fraction of memory T cells (47). They play a major role in lymphocyte homing to LNs, in steady state as well as under conditions of inflammation, and may control T-cell positioning within defined functional compartments (1, 17, 18, 47). CXCR4 and its ligand CXCL12/SDF-1 also contribute to T-cell entry into LNs (5, 23, 40). In addition, effector and memory T cells express a broad range of receptors binding inflammatory chemokines, such as the CCR5 ligands CCL3 (MIP1 α), CCL4 (MIP1 β), and CCL5 (Rantes).

Efficient accomplishment of lymphocyte migration and immune functions requires tight regulation of the cellular cytoskeleton (59). This is mediated by the small GTPases of the Rho subfamily, such as Rho, Rac, and Cdc42 (11, 58). They activate specific actin filament assembly factors to generate sheet-like protrusive structures (such as lamellipodia and ruffles) and finger-like protrusions (such as filopodia and microvilli) (6). These structures have different functions. Lamellipodia and ruffles are formed during crawling cell motility and spreading. Filopodia protrude from the leading edges of many motile cells. They appear to perform sensory and exploratory functions to steer cells, depending on cues from the environment (42). Moreover, filopodia, or other thin structures called

* Corresponding author. Mailing address: Virus and Immunity Unit, Department of Virology, Institut Pasteur, URA CNRS 3015, 28 rue du Dr. Roux, 75724 Paris Cedex 15, France. Phone for O. Schwartz: 330145688353. Phone for N. Sol-Foulon: 330145688783. Fax: 330140613465. E-mail for O. Schwartz: schwartz@pasteur.fr. E-mail for N. Sol-Foulon: nathalie.sol-foulon@pasteur.fr.

† C.N. and D.R. contributed equally to this work as first authors; O.S. and N.S.-F. contributed equally to this work as senior authors.

[∇] Published ahead of print on 16 December 2009.

tunneling nanotubes, have been shown to form intercellular bridges, allowing viruses to spread through remote contacts between infected cells and targets (44, 48, 49, 52).

HIV-1 hijacks cytoskeleton dynamics in order to ensure viral entry and transport within and egress from target cells (34; reviewed in reference 13). In particular, the viral protein Nef modifies actin remodeling in various cell systems. In T cells, Nef alters actin rearrangements triggered by activation of T-cell (TCR) or chemokine receptors (22, 54). Nef inhibits immunological synapse formation, a dynamic process involving rapid actin modifications (57). Nef also affects plasma membrane plasticity, inducing secretion of microvesicle clusters (33). In macrophages, Nef induces the extension of long intercellular conduits allowing its own transfer to B cells (61). A number of studies have reported that Nef affects T-cell chemotaxis (generally to CXCL12) through the modulation of Rho-GTPase-regulated signaling pathways (7, 24, 39, 54). Migration studies have generally been performed using Nef-expressing cells, and rarely in the context of HIV-1 infection (54). From a molecular standpoint, it has recently been proposed that Nef acts in part by deregulating cofilin, an actin-depolymerizing factor that promotes actin turnover and subsequent cell motility (54).

In the present study, our goal was to gain further insights into the effect of HIV-1 infection on cytoskeleton dynamics. We used a panel of innovative techniques allowing analysis of cell shape, adhesion, and motility. We report that in HIV-1-infected lymphocytes, Nef promotes filopodium-like formation while it inhibits membrane ruffling. Nef impairs cell adhesion on the extracellular matrix and decreases intrinsic cell motility. Lymphocyte migration toward various chemokines (CXCL12, CCL3, and CCL19) is also inhibited. Our results suggest that Nef may facilitate viral spread and contribute to AIDS pathogenesis by manipulating the migration of lymphocytes.

MATERIALS AND METHODS

Cells, viruses, and infections. Jurkat cells (clone 20) and peripheral blood mononuclear cells (PBMC) were grown in RPMI 1640 (Invitrogen) supplemented with 10% fetal calf serum (Sigma) and penicillin-streptomycin (100 IU/ml; Sigma). Primary CD4⁺ T cells were isolated after negative sorting of PBMC obtained by Ficol gradient (Amersham Biosciences), using magnetic beads (CD4⁺ T-cell isolation kit II; Miltenyi Biotec). They were stimulated with phytohemagglutinin (PHA) for 48 h and cultured with interleukin 2 (IL-2) (50 IU/ml; Chiron). Jurkat cells stably expressing actin-green fluorescent protein (GFP) were obtained by transfection with a pcDNA3 construct containing a chimeric enhanced GFP (EGFP)-human beta actin chimeric sequence controlled by a cytomegalovirus (CMV) promoter described previously (3). The production and use of wild-type (WT) and Δ nef HIV-1 NL4.3 and NLAD8 strains and WT and mutant (G2A, PP76/79AA, and LL168/169AA) HIV-1 (SF2) Nef have been described (15, 31). For HIV infection, cells were exposed to the indicated virus (viral input, 5 to 20 ng p24/ml/10⁶ cells) for 2.5 h, washed, seeded in 25-cm² flasks, and used few days later.

Use of lentiviral vectors. The pHR⁺Nef lentiviral vector carrying the HIV LAI (also termed R7) *nef* gene (under the control of the elongation factor 1 α promoter) was a kind gift from Didier Trono. The Nef G2A mutant was obtained as described previously (51). Lentiviral vector particle production and the transduction of Jurkat cells were performed as described previously (51).

Flow cytometry and confocal microscopy. Cell surface staining was performed at 4°C for 30 min using monoclonal antibodies (MAbs) directed against the following molecules: CD4 (13B8.2-allophycocyanin [APC]; Beckman Coulter); CXCR4 and CCR5 (12G5 and 2D7; NIH AIDS Research and Reference Reagent Program); CCR7 (150503; R&D systems); and CD29, CD49d, and CD49e (Immuntools). Gag p24 expression in infected cells was measured after permeabilization and intracellular staining with anti-Gagp24-fluorescein isothiocyanate

(FITC) MAb (KC57; Coulter). Isotype-matched MAbs were used as negative controls. Samples were analyzed by flow cytometry using a FACS Calibur (Becton Dickinson) with FlowJo software. For immunofluorescence (IF) studies, infected Jurkat cells were fixed in 4% paraformaldehyde (PFA) for 15 min, permeabilized with phosphate-buffered saline (PBS)-0.2% bovine serum albumin (BSA)-0.05% saponin, and stained with anti-Gag MAbs (25A and 18A; Hybridolabs, Pasteur) or with anti-Nef MAb (MATG020; Transgene [Strasbourg, France]) and with rhodamine-phalloidin, a high-affinity probe for F-actin (Invitrogen). Confocal microscopy analysis was carried out on a Zeiss LSM510 using a 63 \times objective. Z series of optical sections were performed in 0.2- to 0.5- μ m increments for qualitative analysis. Green and red fluorescence were acquired sequentially to prevent passage of fluorescence from one channel into the other.

Image Stream flow cytometer (Amnis). Uninfected WT- and Δ nef-infected Jurkat cells were fixed, permeabilized, and stained with phalloidin-FITC (Molecular Probes, Invitrogen) and mouse anti-Gag Ab (25A and 18A; Hybridolabs, Institut Pasteur), followed by anti-mouse Cy5 Ab (Jackson ImmunoResearch). DAPI (4',6'-diamidino-2-phenylindole) (Invitrogen) was used to visualize cellular nuclei. Five thousand cells were acquired for each sample, and digital imaging was performed on a multispectral imaging flow cytometer (ImageStream100; Amnis Corporation, Seattle, WA). The data were analyzed using the manufacturer's software (IDEAS; Amnis Corporation). Briefly, fluorometric compensation was digitally calculated based on single-stain controls. The single cells and cells in focus were selected based on a digital plot of aspect ratio with area and of the gradient root mean square (RMS) of bright-field images, respectively. An object mask based on DAPI staining was created to define the nuclear region. The apoptotic cells were excluded using an area of 40% threshold mask and bright detail intensity R3 features, both calculated on the nuclear mask. Infected cells (Gag⁺) and cells positive for phalloidin staining were identified by the intensity of fluorescence signals. A morphology mask based on phalloidin staining was created to define cell shape. The algorithm used to separate cells by their shapes included a calculation of symmetry 3 and circularity features on this morphology mask. A digital plot of these two features enabled drawing of gates to separate circular cells from cells bearing protrusions.

SEM. For scanning electron microscopy (SEM), cells were loaded on a polylysine-coated coverslip and fixed with 0.1% glutaraldehyde (GA)-4% PFA in 0.1 M Sorensen buffer for 30 min at 4°C. The cells were then incubated successively in PBS-0.25% NH₄Cl for 20 min and PBS-1% BSA for 30 min, followed by incubation with anti-Gp120 Ab for 1 h. Subsequently, they were incubated for 1 h with an anti-mouse Ab conjugated to 20-nm colloidal gold particles (British Biocell International). The cells were fixed in 2.5% GA in 0.1 M cacodylate buffer (pH 7.2) overnight at 4°C and postfixed for 1 h in 1% OsO₄ in 0.2 M cacodylate buffer (pH 7.2). Samples were dehydrated, followed by critical-point drying with CO₂. The specimens were mounted on stubs with carbon tape and ion sputtered with carbon using a Gatan 681 high-resolution ion beam coat. Analysis of the secondary electron image (SEI) and backscattered images (YAG detector) was performed on a JSM 6700F Jeol microscope with a field emission gun operating at 5 kV. Images were acquired simultaneously from the upper secondary electron detector and the YAG backscattered electron detector.

Three-dimensional (3D) imaging microscopy of living cells in suspension. We used a novel methodological approach called "automation," which allows visualization and axial tomography of living Jurkat cells expressing actin-GFP. Cells were resuspended in Cytocon buffer II (Evotec Technologies/Perkin Elmer) at a final concentration of 10⁶ cells/ml. Analysis was performed on single cells immobilized in a cage by a dielectric field and then visualized by high-resolution confocal microscopy as described previously (41).

Live imaging. The shapes of living Jurkat cells were analyzed on a microdish (Ibidi, Germany) precoated with 10 μ g/ml fibronectin (Sigma). Images were acquired every 10 s for up to 15 min. Data acquisition was done on an Axiovert 200 M (Zeiss, Germany) equipped with an ultraview RS Nipkow spinning-disk system (Perkin Elmer) and a camera (Hamamatsu Orca II ER).

Adhesion assays. Cells were counted and distributed in 96-well plates (Greiner BioOne) coated with fibronectin (10 μ g/ml). After 30 min at 37°C, nonadherent cells were removed and adherent cells were fixed, permeabilized, and stained with phalloidin-FITC and Hoechst stain to visualize nuclei, as described for IF studies. An automated high-content imaging system (Opera QEHS; Perkin Elmer) was used to acquire images of entire wells. The evaluation of the total number of cells per well was done using a dedicated software script (Acapella; Perkin Elmer) outputting the number of objects found in the Hoechst channel.

Migration assays. Chemotaxis of Jurkat cells and activated CD4⁺ T cells was measured by migration through a polycarbonate filter of 5- μ m pore size in transwell chambers (Corning Costar, Lowell, MA). Cells (4 \times 10⁵; 150 μ l) were seeded in the upper chamber, and control medium or stimuli (250 μ l of recombinant chemokines) were added to the lower chamber. In order to determine the

optimal chemokine dose inducing T-cell migration, various concentrations were tested. We obtained a dose-response curve for each chemokine, and experiments were then performed using a dose below the plateau, e.g., CXCL12/SDF-1 (3 nM) and CCL19 and CCL3 (100 ng/ml) (R&D Systems). After incubation at 37°C, 10^5 beads (Beckman Coulter, Villepinte, France) were added to all lower wells, and the number of cells for a given number of beads was determined by flow cytometry. The values are given as the number of cells in the lower well/total number of cells (n). In experiments with infected cells, Gag staining was performed on cells before and after migration, and the data are represented as percentage of migration of the Gag^+ and the Gag^- populations [% migration ($\text{Gag}^+/\text{Gag}^-$) = migrated ($\text{Gag}^+/\text{Gag}^-$)/ n ($\text{Gag}^+/\text{Gag}^-$)].

RESULTS

Nef alters cell shape and induces filopodia in HIV-1-infected lymphocytes. We examined the shape of HIV-infected lymphocytes. Jurkat cells were infected with HIV NL4.3 (WT) and analyzed 2 to 3 days later, when about 50% of the cells expressed Gag antigens. Productively infected cells were visualized by SEM after anti-Env immunogold staining and detection of viral particles (Fig. 1A) or by confocal immunofluorescence after Gag and actin staining (Fig. 1B). In control noninfected cells, large ruffles, defined as actin-rich sheet-like membrane protrusions, were visible. In contrast, HIV-infected cells often displayed a round shape with fewer and smaller ruffles. Moreover, infected cells emitted numerous filopodia, finger-like protrusions that were generally adherent to the substratum.

To examine the role of Nef in cell shape changes, Jurkat cells were infected with HIV with *nef* deleted (Δnef). WT and Δnef HIV replicated similarly and led to the same levels of Gag expression (reference 51 and data not shown) in Jurkat cells. However, the shape and membrane-ruffling activity of Δnef -infected cells were apparently normal at day 3 postinfection (p.i.) (Fig. 1A and B) and at earlier time points (not shown).

We quantified by visual examination the number of cells presenting different types of protrusions (Fig. 1C). Noninfected (NI) lymphocytes presented large ruffles (80% of the cells) and rarely filopodia (10%). This repartition was similar with Δnef -infected cells: 70% of them displayed ruffles and rarely filopodia (10%). In contrast, 40% of WT HIV-infected cells formed no protrusions, and 25% expressed several filopodia. Similar results were obtained at different time points after infection, suggesting that the changes were not due to a pleiotropic viral cytopathic effect (data not shown).

The filopodia were frequently decorated with Gag^+ spots (Fig. 1B) (44) that likely corresponded to virions being transported to the tips of the cells. The filopodia also often established contacts with neighboring infected or noninfected cells (Fig. 1B and not shown). Nef localized as expected to the plasma membrane and in a perinuclear region likely corresponding to the Golgi apparatus and endocytic compartment but was also detected inside these filopodia (Fig. 1D), confirming recent observations in macrophages (61). Therefore, the presence of Nef in infected lymphocytes induces these cell conduits, where the viral protein accumulates.

Nef exerts multiple activities involving various regions of the viral protein. We examined which domains of Nef are implicated in cell shape remodeling. Jurkat cells were infected with HIV expressing either a WT Nef or proteins carrying mutations either in the myristoylation domain (Nef G2A), in the dileucine motif required for CD4 down-mod-

ulation (Nef LL168/169AA), or in the SH3-like proline-rich region modulating interaction with various kinases (Nef PP76/79AA). We used recombinant HIV carrying the Nef SF2 allele (15). Nef SF2 also induced rounding of the cell and the appearance of filopodia (Sup. Fig. 1 at <http://www.pasteur.fr/ip/easysite/go/03b-00003g-063/virus-and-immunity/supplemental-material>). Mutations of the myristoylation motif that affects Nef association with vesicular and plasma membranes, and of the SH3-binding domain (PP76/79AA), abolished cell shape modifications. In contrast, the LL168/169AA mutant that no longer interacted with the cell-sorting machinery behaved like the WT protein (Sup. Fig. 1 at <http://www.pasteur.fr/ip/easysite/go/03b-00003g-063/virus-and-immunity/supplemental-material>). Thus, Nef-induced actin remodeling is observed with different viral strains (NL43 and SF-2) and requires association of the viral protein with cellular membranes and the correct conformation of its SH3-binding domain.

We then used an automated method to examine the morphology of infected cells. The ImageStream system (Amnis) combines flow cytometry with intracellular imaging and localization of fluorescent molecules (36). It enables qualitative and quantitative assessment of the morphology of a high number of cells (a few thousand per sample). We first analyzed NI Jurkat cells to define the parameters allowing the discrimination of circular cells, with no protrusions, from those expressing cellular protrusions or ruffles. Cells were fixed, stained with phalloidin to visualize the actin cytoskeleton, and analyzed. The gating strategy, as well as representative cells with different morphologies, is depicted in the supplemental material (Sup. Fig. 2 at <http://www.pasteur.fr/ip/easysite/go/03b-00003g-063/virus-and-immunity/supplemental-material>). This technique allowed us to readily distinguish round cells from those displaying ruffles on their surfaces. Filopodia could not be visualized, probably because they are too thin and fragile. We then compared the morphology of NI cells to that of HIV WT- and Δnef -infected cells at day 3 p.i. After fixation, Gag staining allowed gating on infected cells (Fig. 2A). Examples of the morphology of infected cells are shown in Fig. 2B. A quantitative analysis confirmed that most NI cells, as well as Δnef -infected cells (about 80% of the cells), expressed ruffles, whereas cells infected with WT HIV were circular (50%) or formed protrusions (50%). Similar results were obtained at earlier or later times postinfection (not shown). Of note, the total amount of filamentous actin, assessed by measuring the intensity of phalloidin staining (Fig. 2A), was not modified in infected cells, strongly suggesting that Nef does not inhibit the actin polymerization process.

The combined analysis of cell morphology by SEM, classical confocal microscopy, and ImageStream indicated that Nef increases the number of filopodia and inhibits ruffle formation, highlighting the fact that Nef may regulate specific actin filament assembly pathways.

Nef is necessary and sufficient to induce filopodia. We asked whether Nef, when expressed alone, is sufficient to modify T-cell shape. To this end, Jurkat cells were transduced with lentiviral vectors expressing WT Nef or the nonmyristoylated Nef G2A mutant. Nef expression, monitored by IF, was observed in more than 90% of cells (not shown). As expected, the presence of WT Nef induced CD4 downregulation from the cell surface (not shown). SEM and IF analyses indicated that

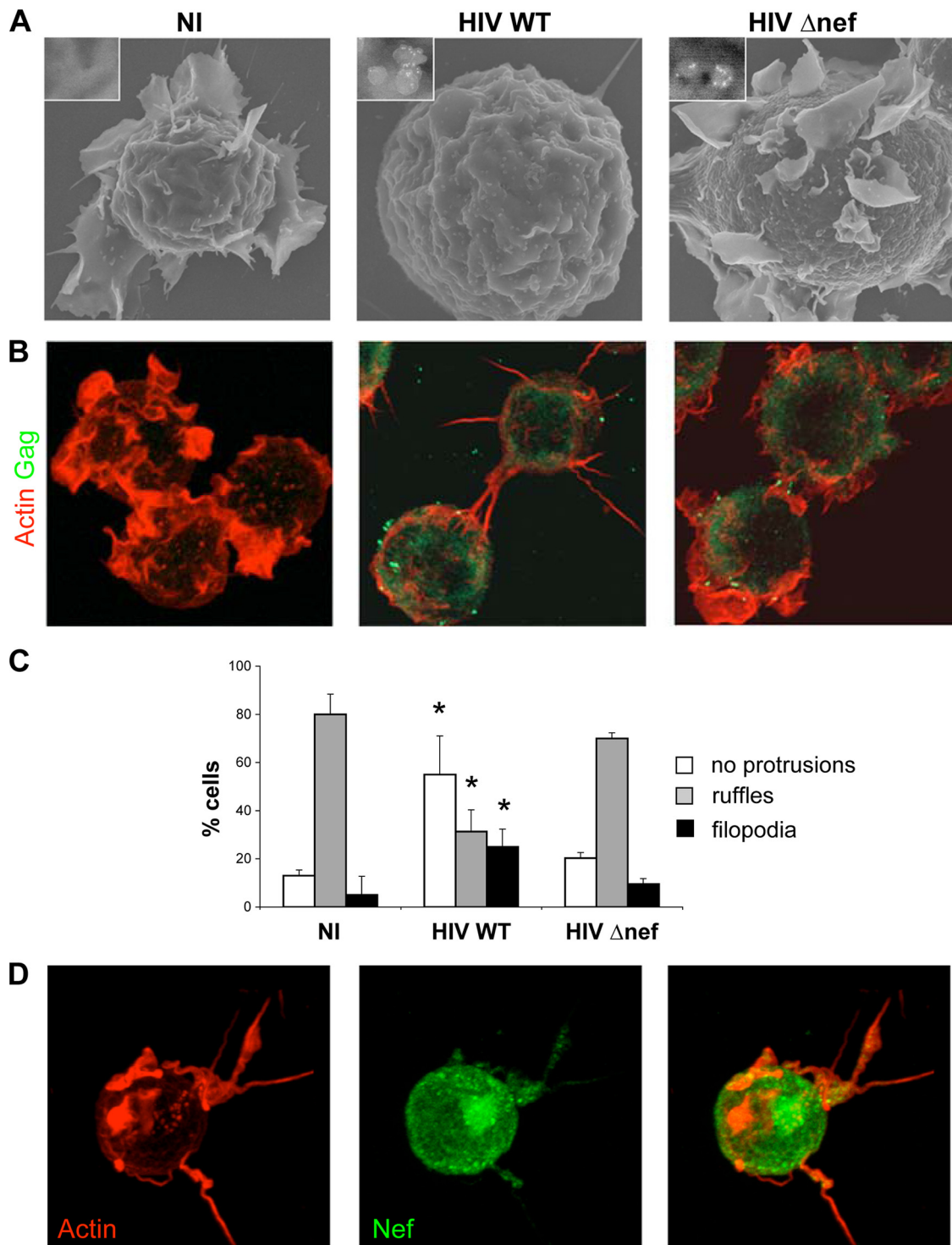


FIG. 1. HIV-1 alters the shape of T lymphocytes through Nef expression. Shown are representative images of NI or HIV WT- or Δ nef-infected Jurkat cells. (A) SEM images. HIV virions were stained with anti-Env MAb coupled to gold particles (appearing as white dots). Insets, higher magnifications of cellular regions showing virus-like particles. (B) 3D reconstruction of confocal images. Cells were stained with phalloidin-rhodamine (red) and anti-Gag MAb (green). (C) Cells without protrusions or with ruffles or filopodia were scored by visual counting under a fluorescence microscope. The data are means plus standard deviations (SD) of four independent experiments, with a total of 415 NI, 337 HIV WT-, and 296 HIV Δ nef-infected cells scored. Significance was assessed by the Mann-Whitney test (*, $P < 0.05$). (D) Nef accumulates in filopodia. Shown is a 3D reconstruction of a representative confocal image. HIV-infected cells were stained with phalloidin-rhodamine (red) and anti-Nef MAb (green).

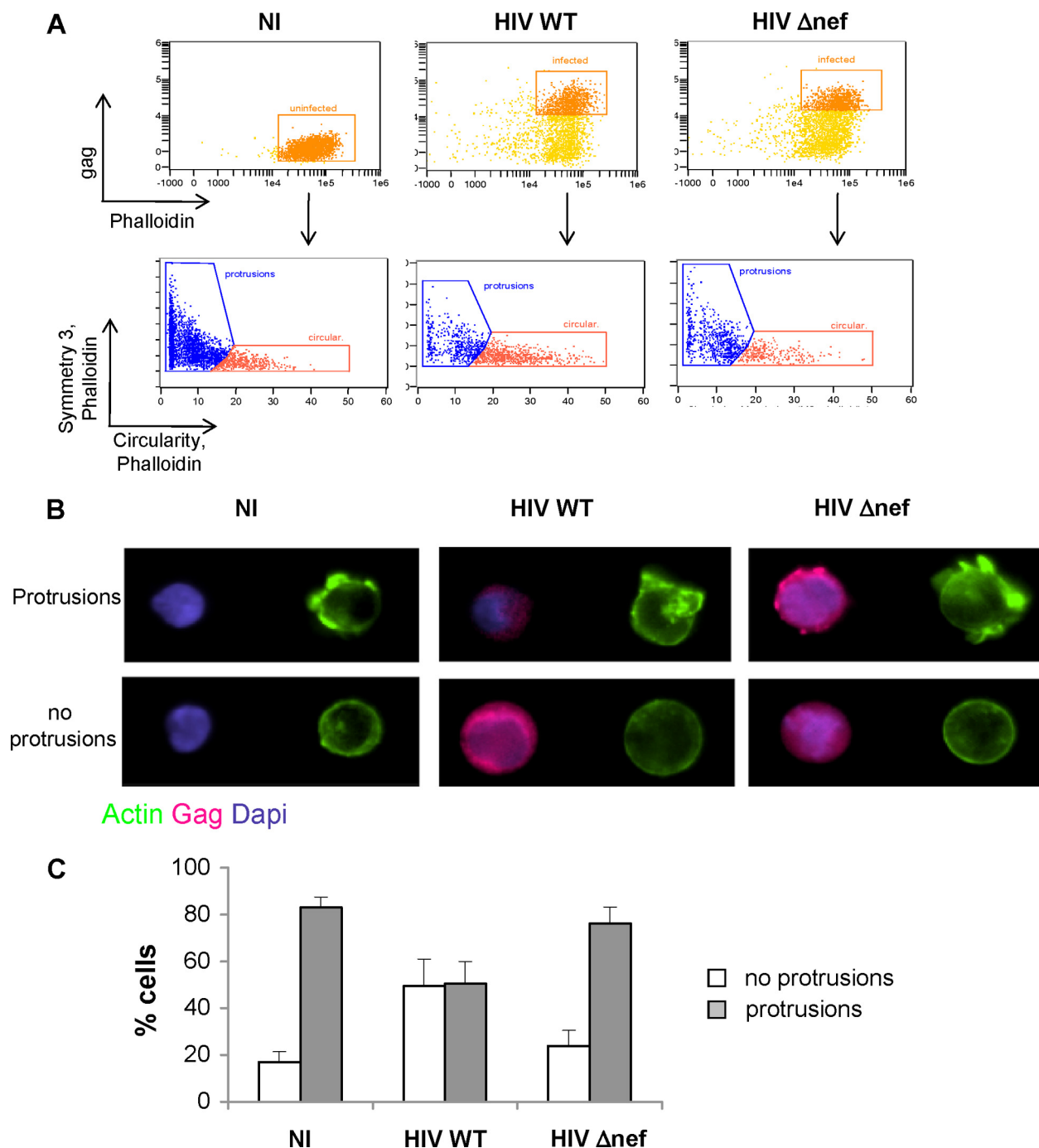


FIG. 2. Automated quantification of T-cell protrusions. Uninfected (NI) or HIV WT- or Δ nef-infected Jurkat cells were stained with anti-Gag MAbs and with phalloidin. Nuclei were visualized with DAPI. Automated quantification of cell shape changes on gated cells was performed using ImageStream technology. (A) Uninfected (Gag^-) or infected (Gag^+) cells, 40.7% for HIV WT and 35.6% for HIV Δ nef, were gated and analyzed by symmetry 3 and circularity features, as detailed in the supplemental material (Sup. Fig. 1 at <http://www.pasteur.fr/ip/easysite/go/03b-00003g-063/virus-and-immunity/supplemental-material>). When plotted together, these two features enable identification and gating of circular cells versus cells with protrusions. (B) Representative images of circular cells and cells with protrusions, identified in panel A. (C) Quantitative analysis of images from these two populations was performed. The percentages of cells with protrusions and circular cells were quantified automatically with IDEAS software. The data represent means and SD of five independent experiments.

ruffle formation was greatly reduced in Nef-expressing cells (from 80% to 20%), whereas filopodia were increased (from 5 to 15%) compared to nontransduced (NT) cells (Fig. 3). In contrast, cells expressing the G2A mutant (Fig. 3) or trans-

duced with a lentivirus encoding GFP (not shown) behaved like NT cells.

Filopodia and other thin membrane protrusions are relatively sensitive to PFA fixation (46); therefore, we may under-

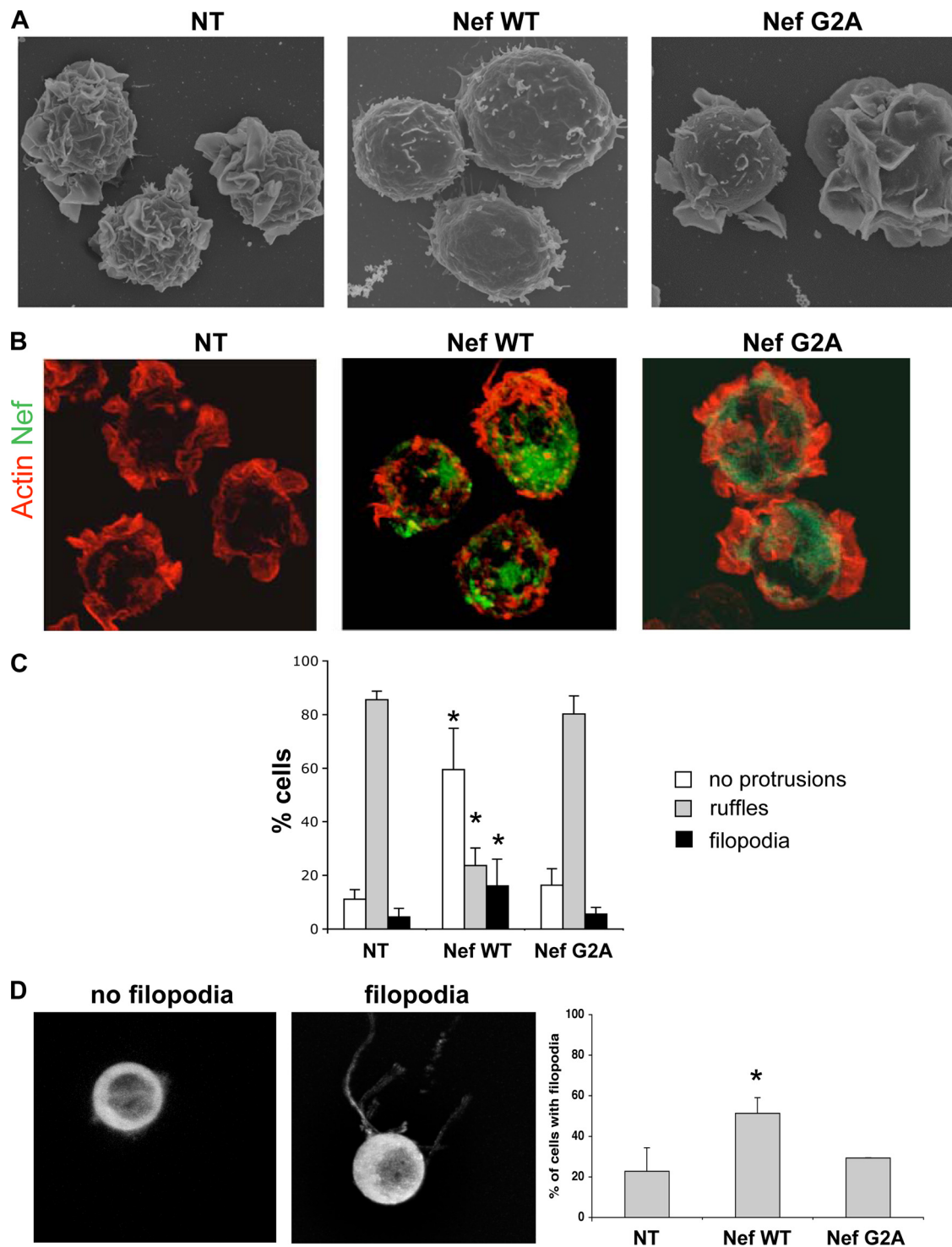


FIG. 3. Nef inhibits ruffles and increases filopodia. (A and B) Representative images of NT Jurkat cells (left) and of cells transduced with lentiviral expression vectors encoding the WT (middle) or the G2A mutant (right). (A) SEM images. (B) 3D reconstruction of confocal images. Cells were stained with phalloidin-rhodamine (red) and anti-Nef MAb (green). (C) Cells without protrusions, with ruffles, or with filopodia were scored by visual counting under a fluorescence microscope, with a total of 235 NT and 235 Nef WT- and 242 Nef G2A-expressing cells analyzed. The data are means and SD of four independent experiments. Significance was assessed by the Mann-Whitney test (*, $P < 0.05$). (D) High-resolution 3D imaging of living cells in suspension. Actin-GFP Jurkat cells transduced with WT- or G2A Nef-expressing vectors were analyzed. Nontransduced cells were used as controls. Representative images of cells with or without filopodia are shown. The data are means and SD of three independent experiments, with about 60 cells analyzed for each condition. Significance was assessed by the Mann-Whitney test (*, $P < 0.05$).

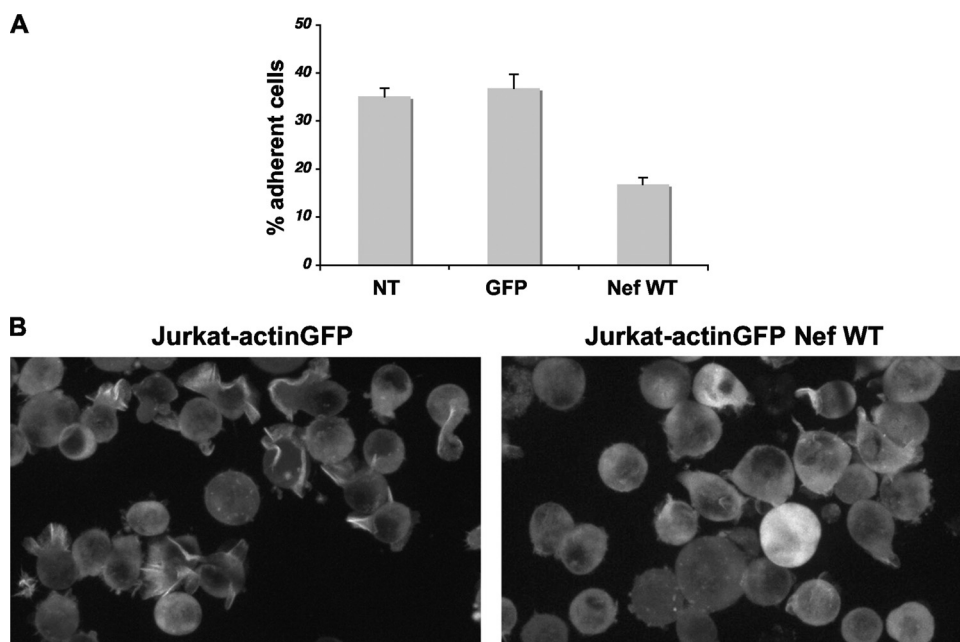


FIG. 4. Nef impairs T-cell adhesion to fibronectin. (A) Quantification. Jurkat cells, NT or transduced with Nef WT or GFP, were left adhering to a fibronectin-coated surface for 30 min. The number of bound cells was determined with an automated system (Opera). The percentages of adherent cells are shown. The data are means and SD of four independent experiments. (B) Visualization of cells by time-lapse videomicroscopy. Control (left) and Nef-expressing actin-GFP (right) Jurkat cells were seeded on fibronectin-coated surfaces. The images are snapshots taken from the supplemental movies (<http://www.pasteur.fr/ip/easysite/go/03b-00003g-063/virus-and-immunity/supplemental-material>) and are representative of three independent experiments.

estimate their numbers in fixed Jurkat cells. We thus explored the effect of Nef on T-cell shape in unfixed, living cells. We used a novel methodological approach, which allows visualization and axial tomography of living cells in suspension (41). A single living cell is immobilized in a cage by an electric field and then analyzed by high-resolution confocal microscopy. To visualize the shapes of the cells, we used Jurkat cells stably expressing an actin-GFP fusion protein. By performing high-resolution 3D imaging, we distinguished cells forming thin and long membrane extensions from those in which these filopodia were absent (Fig. 3D). Jurkat actin-GFP cells were then transduced with lentiviral vectors encoding WT or G2A Nef, and the presence of the viral protein was assessed by immunofluorescence (not shown). We observed that more than 50% of cells expressing WT Nef were forming filopodium-like structures, whereas this was the case in only 20% of NT or Nef G2A-positive cells. The number and length of filopodia were higher in unfixed living cells than in fixed cells, confirming that these structures are fragile. Of note, this technique did not allow the visualization of large ruffles, probably because the cells are immobilized in suspension in an electric field.

Taken together, our results show that Nef by itself changes the morphology of and induces filopodia in Jurkat cells.

Impact of Nef on T-cell adhesion to fibronectin. We asked whether the reorganization of the actin cytoskeleton induced by Nef resulted in impaired interaction of lymphocytes with the extracellular matrix. We studied the ability of T cells, expressing Nef or GFP as a control, to adhere to fibronectin-coated surfaces. The percentage of adhesion was calculated by using an automated confocal microplate imaging reader

(Opera). Adhesion to fibronectin was reduced by 50% in Nef-positive cells compared to NT or GFP-positive cells (Fig. 4A). Of note, the inhibitory effect of Nef on cell adhesion was not due to reduced surface expression of $\alpha 4\beta 1$ (VLA-4) and $\alpha 5\beta 1$ integrins (<http://www.pasteur.fr/ip/easysite/go/03b-00003g-063/virus-and-immunity/supplemental-material>, Fig. 3), which are known to mediate cell binding to fibronectin.

We next examined the impact of Nef on the dynamic interactions of T cells with fibronectin by performing real-time imaging of living cells. Jurkat actin-GFP cells were transduced with Nef or with a control vector. The cells were then plated on coverslips coated with fibronectin and visualized by time-lapse videomicroscopy. Images were acquired every 10s for up to 15 min. Two representative examples are shown in supplemental movie 1 (control cells) and movie 2 (Nef-expressing cells) (<http://www.pasteur.fr/ip/easysite/go/03b-00003g-063/virus-and-immunity/supplemental-material>). Control cells were generally mobile and dynamically extended and retracted large ruffles (Fig. 4B; see supplemental movie 1 [<http://www.pasteur.fr/ip/easysite/go/03b-00003g-063/virus-and-immunity/supplemental-material>]). Nef-positive cells were less mobile. These cells showed impaired ruffle formation and spreading, whereas transient filopodium-like structures were visible (Fig. 4B; see supplemental movie 2 [<http://www.pasteur.fr/ip/easysite/go/03b-00003g-063/virus-and-immunity/supplemental-material>]), confirming the results depicted above, obtained in fixed cells. Therefore, Nef expression strongly reduces cell spreading and adhesion to extracellular matrix.

Nef impairs intrinsic motility and CXCL12 chemotaxis of Jurkat cells. The modifications of the actin cytoskeleton dy-

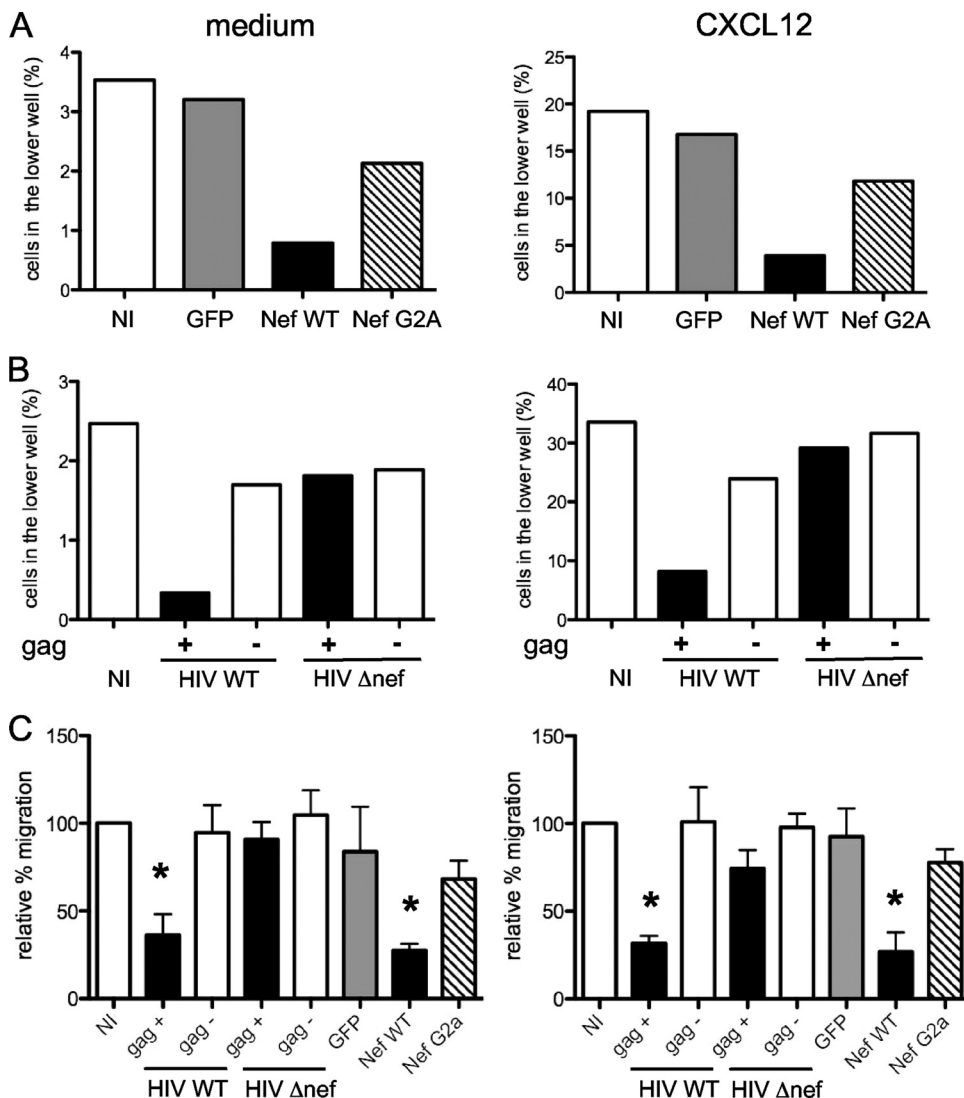


FIG. 5. Nef alters T-cell intrinsic motility and chemotaxis to CXCL12 (SDF-1). Shown are transwell chemotaxis assays. Jurkat cells were placed in the upper chamber of a transwell and medium or chemokines in the lower chamber. The percentages of T cells attracted to the medium after 4 h or to CXCL12 after 2 h were calculated. (A and B) Representative experiments. (A) Cells transduced with control GFP, Nef WT, or Nef G2A. (B) Cells infected with HIV or HIV Δnef. (C) The data were normalized to the percentage of migration of noninfected cells (100%). The means and standard errors of the mean of four independent experiments are shown. Significance was assessed by a Mann-Whitney test (*, $P < 0.05$).

namics are likely associated with altered movements of infected cells. To explore the impact of Nef on T-cell motility, we performed transwell migration assays. We first examined the “intrinsic motility” of Jurkat cells, e.g., their ability to move in the absence of stimuli. Jurkat cells expressing WT or G2A Nef, or GFP as a control, were incubated in a transwell chamber for 4 h in medium without chemokines, and the fraction of cells that migrated spontaneously across the membrane was measured. About 4% of nontransduced cells, or of control GFP-expressing cells, moved during this time (Fig. 5A). Nef-positive cells were less motile, with a 4-fold decrease in the fraction of cells spontaneously crossing the membrane (Fig. 5C). Nef G2A-positive cells showed a slight decrease in migration (Fig. 5A and C). We then investigated if Nef affected chemotaxis toward CXCL12 (SDF-1). To determine the optimal dose of CXCL12, we tested various concentrations of the chemokine

on Jurkat migration. We obtained a dose-response curve, and experiments were then performed using a “subsaturating” dose, e.g., a dose below the plateau.

The presence of CXCL12 strongly induced Jurkat migration, with 20% of the cells crossing the membrane in 2 h (Fig. 5A). Nef inhibited CXCL12-induced chemotaxis (Fig. 5A), again with a 4-fold decrease in migration (Fig. 5C). As for intrinsic motility, control GFP-expressing cells moved normally, whereas Nef G2A slightly impaired Jurkat cell motility (Fig. 5A and C).

We next studied the effect of Nef on lymphocyte migration in the context of infected cells. To this end, Jurkat cells were infected at similar levels with WT or Δnef HIV. The percentage of Gag⁺ cells was then determined by fluorescence-activated cell sorter (FACS) analysis before and after migration in the lower chamber, allowing quantification of the migration of

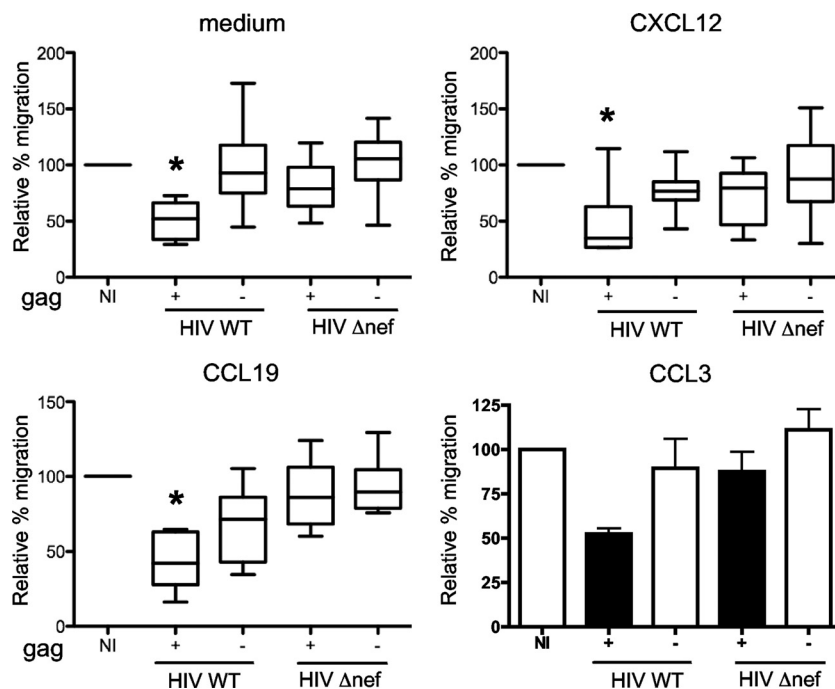


FIG. 6. Nef inhibits chemotaxis of primary T cells to CXCL12, CCL19, and CCL3 in transwell chemotaxis assays. Blasts were placed in the upper chamber of a transwell and medium or chemokines in the lower chamber. The percentages of T cells attracted to the lower chamber after 1 h are shown. For each condition, the data were normalized to the percentage of migration of noninfected cells (100%). The medians and interquartile ranges of 7 independent experiments are shown for all conditions except CCL3. For CCL3, the data are means and SD of two independent experiments. Significance was assessed by a Mann-Whitney test (*, $P < 0.05$).

both infected (Gag^+) and NI (Gag^-) populations. With the WT virus, migration of Gag^+ cells toward the medium or toward CXCL12 was drastically decreased compared to NI or Δnef -infected cells (Fig. 5B and C). Interestingly, the Gag -negative cells present in the population of WT or Δnef -infected cells migrated normally (Fig. 5B and C), indicating that HIV does not significantly affect the motility of bystander noninfected cells.

Altogether, these results indicate that Nef, expressed alone or in the context of infection, strongly inhibits intrinsic motility and CXCL12-induced T-cell migration.

Nef impairs the motility of primary $CD4^+$ lymphocytes. We then measured the motility of HIV-infected primary $CD4^+$ lymphocytes. Primary lymphocytes, but not Jurkat cells, express CCR7 (the receptor for CCL19 and CCL21) and CCR5 (the receptor for CCL3, CCL4, and CCL5). $CD4^+$ lymphocytes were infected with WT or Δnef HIV (strain NL43), and 2 to 3 days later, when about 15 to 40% of the population expressed Gag antigens, we measured chemotaxis toward CXCL12, CCL19, and CCL3. HIV-1 infection did not modify CXCR4, CCR7, or CCR5 surface levels (not shown). The motility of primary $CD4^+$ cells is higher than that of Jurkat cells. We thus performed 1-h transwell migration assays. Under these conditions, using subsaturating doses of chemokines, we could observe T-cell chemotaxis toward CXCL12, CCL19, and CCL3 (20%, 50%, and 50%, respectively, of the cells migrated, whereas only 10% of the cells migrated in medium alone).

The results from seven different donors are compiled in Fig. 6. We first verified that noninfected cells responded to the

chemokines. We observed a 2- to 5-fold increase in cell migration, depending on the chemokines (not shown). We then examined the intrinsic motility of infected cells. In the absence of any chemokines, migration was reduced in cells infected with WT HIV and not in cells infected with Δnef HIV, which behaved like noninfected cells (Fig. 6). Similarly, HIV infection impaired chemotaxis toward CXCL12, CCL19, and CCL3, only in the presence of Nef (Fig. 6).

Altogether, these results indicate that Nef inhibits intrinsic motility, as well as migration toward various chemokines (CXCL12, CCL19, and CCL3), in Jurkat cells and in primary lymphocytes.

DISCUSSION

We explored the effect of HIV-1 on the shape and motility of $CD4^+$ T cells by combining various techniques (scanning electron microscopy, immunofluorescence confocal microscopy, automated flow cytometry imaging with the Amnis apparatus, and live-cell imaging). We reported that HIV-1, through expression of Nef, profoundly alters the morphology of infected T cells. Nef decreases ruffle protrusions but promotes the formation of filopodium-like structures. The total amount of F-actin is apparently not modified by Nef, as assessed by Amnis analysis, suggesting that the viral protein does not inhibit polymerization but rather alters actin remodeling. Nef likely modulates regulators of actin assembly pathways, leading to the formation of these long, thin membrane extensions instead of ruffles. It has been suggested that ruffle formation involves Arp2/3 complex-generated dendritic networks

while filopodia assemble by “convergent elongation” of actin filaments (6). We can speculate that Nef alters the formation of ruffles through interaction with Arp2/3, promoting the formation of unbranched actin filaments, leading to filopodium extension. The phenotype induced by Nef is indeed reminiscent of that observed in Arp2-depleted lymphocytes (35), which exhibit defects in ruffle assembly and remain covered with finger-like protrusions. To better understand how these morphological changes are induced, we used HIV-1 expressing Nef proteins mutated in different functional domains (15). The effect of Nef is dependent on its myristoylated motif and SH3-binding domain. Myristoylation, and hence membrane association, is required for most known activities of Nef. The proline-rich SH3-binding domain is involved in Nef association with Vav, DOCK2-ELMO1, and Pak2 (p21-activated kinase 2) and Nef-induced activation of Rac and Pak2 (14, 22, 24, 30). Pak2 activation promotes phosphorylation of cofilin (54) and has been proposed to mediate Nef-induced inhibition of actin rearrangements (22, 54). It will be worthwhile to determine, by using a large panel of Nef mutants, the domains of Nef responsible for filopodium induction, as well as to identify the actin regulators involved, such as Pak2 and Arp 2/3.

The filopodium development induced by Nef may enhance communication and the exchange of cellular or viral materials between infected lymphocytes and bystander cells and may facilitate viral transfer to other cells. HIV-1 efficiently propagates through cell-to-cell contacts, mainly through virological synapse and polysynapse formation, and also by establishing remote connections via filopodial bridges or nanotubes (25, 44, 48, 52). Cell-to-cell viral spread is dependent on actin rearrangements (26, 44). HIV-1 infection of macrophages also enhances filopodium formation and transfer of Nef to neighboring B cells via long-range intercellular conduits (12, 61, 45). We showed here that Nef is also found within T-cell filopodia, suggesting it could be similarly delivered from infected lymphocytes to bystander immune or nonimmune cells. Interestingly, Nef transfer between T cells may also occur through exchange of microvesicles or patches of plasma membrane (33). Altogether, these results indicate that Nef uses various means to perturb intercellular communication networks.

We further documented the consequences of Nef expression for actin-dependent processes by studying adhesion to extracellular matrix. We showed that Nef expression reduces T-cell adhesion to fibronectin-coated surfaces. After binding to fibronectin, Nef-expressing T cells displayed impaired ruffling activity and spreading, as visualized by real-time imaging. Nef does not alter surface expression of $\alpha 4\beta 1$ and $\alpha 5\beta 1$ integrins that bind fibronectin. Adhesion of T cells to the extracellular matrix is controlled by a modulation of the affinity of integrins and involves actin cytoskeleton rearrangements and cell spreading (43). Rac and Lck regulate integrin-mediated spreading and adhesion of T cells (9, 16, 19). The intracellular distribution of Lck is modified by Nef (57). The adhesion defect of T cells may thus in part result from Nef-induced perturbation of Lck and Rac proteins (4, 24). The impaired adhesion to fibronectin suggests that infected lymphocytes may not correctly bind to HEV, the first step of the extravasation process, and helps to explain why transendothelial migration of Nef-expressing cells is decreased in culture systems (39). It will

be worthwhile to further study the interaction of infected lymphocytes with endothelial cells.

We demonstrated here that Nef inhibits the intrinsic motility of infected T cells. Lymphocytes move by a mechanism that involves contractility of the actomyosin cortex (38, 59). Our results suggest that Nef globally alters this process, probably as a consequence of the morphological changes described above. We also reported, using Nef-transduced or HIV-infected Jurkat cells, that Nef inhibits T-cell chemotaxis toward CXCL12, thus confirming previous reports (7, 24, 39, 54). We extended these observations by showing that primary lymphocyte motility toward a variety of chemokines controlling homing to LNs (CXCL12, CCL19, and CCL3) is also impaired. A recent work indicated that Nef inhibits morphological changes induced by chemokines, providing a link between actin rearrangements induced by Nef and inhibition of motility (54).

The viral envelope glycoprotein (gp120) also interferes with chemokine-receptor or CD4 signaling pathways (2, 20, 62). The combined effect of Nef and Env on the behavior and motility of lymphocytes in culture experiments is probably highly relevant to the *in vivo* situation. Studies of the dynamics of HIV-1 infection in lymphoid tissues, after initiation of antiretroviral therapy, identified two populations with different turnovers: activated CD4⁺ T cells (with a half-life [$t_{1/2}$] of 1 to 2 days) and resting or low-level-proliferating T cells ($t_{1/2}$ = 14 days) (8, 50), which constitute a long-term reservoir. Expression of Nef in acutely infected activated cells, but also in these long-living T cells, could modulate their migration capacity. During chronic HIV infection, LNs are often enlarged and inflammatory and are characterized by dramatic lymphocyte sequestration (27). In monkey lymphoid tissues, WT simian immunodeficiency virus (SIV)-infected and Δnef SIV-infected cells accumulate in different zones (55), suggesting that Nef may affect cell migration *in vivo*. T cells, once infected by HIV within LNs, might display defective migration properties, which could explain their sequestration, as well as their different localization, within these organs. In summary, Nef displays complex effects on the lymphocyte actin cytoskeleton and cellular morphology, which likely impact the capacity of infected cells to recirculate and to encounter and communicate with antigen-presenting cells (APCs) and other cells and to disseminate infection.

ACKNOWLEDGMENTS

We thank Maria-Isabel Thoulouze, Françoise Bachelierie, and the members of the GVI laboratory for discussions and critical reading of the manuscript; Pierre-Henri Commere, Emmanuelle Perret, Pascal Roux, Anne Danckaert, and Spencer Shorte (Institut Pasteur, Imagopole) for support in image acquisition and analysis; Stephanie Guadagnini for electron microscopy analysis, Françoise Bachelierie and the NIH AIDS Research and Reference Reagent Program for the kind gift of reagents; and Sherree Friend from Amnis Corporation for her advice on the choice of algorithms for Image Stream data analysis.

This work has been supported by grants from Agence Nationale de Recherche sur le SIDA (ANRS), Sidaction, CNRS, European Community (FP7 contract 201412), Conseil de la Region Ile-de-France (program Sesame 2007, project Imagopde, Spencer Shorte), and the Institut Pasteur. C.N. is a postdoctoral fellow of Sidaction. D.R. is supported by a Marie Curie fellowship (FP6 contract, INTRAPATH program).

REFERENCES

- Asperti-Boursin, F., E. Real, G. Bismuth, A. Trautmann, and E. Donnadieu. 2007. CCR7 ligands control basal T cell motility within lymph node slices in a phosphoinositide 3-kinase-independent manner. *J. Exp. Med.* **204**:1167–1179.
- Balabanian, K., J. Harriague, C. Decrion, B. Lagane, S. Shorte, F. Baleux, J. L. Virelizier, F. Arenzana-Seisdedos, and L. A. Chakrabarti. 2004. CXCR4-tropic HIV-1 envelope glycoprotein functions as a viral chemokine in unstimulated primary CD4⁺ T lymphocytes. *J. Immunol.* **173**:7150–7160.
- Ballestrem, C., B. Wehrle-Haller, and B. A. Imhof. 1998. Actin dynamics in living mammalian cells. *J. Cell Sci.* **111**:1649–1658.
- Baur, A. S., G. Sass, B. Laffert, D. Willbold, C. Cheng-Mayer, and B. M. Peterlin. 1997. The N-terminus of Nef from HIV-1/SIV associates with a protein complex containing Lck and a serine kinase. *Immunity* **6**:283–291.
- Bleul, C. C., M. Farzan, H. Choe, C. Parolin, Y. Clarck-Lewis, J. Sodroski, and T. A. Springer. 1996. The lymphocyte chemo-attractant SDF-1 is a ligand for lestr/fusin and blocks HIV-1 entry. *Nature* **382**:829–833.
- Chhabra, E. S., and H. N. Higgs. 2007. The many faces of actin: matching assembly factors with cellular structures. *Nat. Cell Biol.* **9**:1110–1121.
- Choe, E. Y., E. S. Schoenberger, J. E. Groopman, and I. W. Park. 2002. HIV Nef inhibits T cell migration. *J. Biol. Chem.* **277**:46079–46084.
- Chomont, N., M. El-Far, P. Ancuta, L. Trautmann, F. A. Procopio, B. Yassine-Diab, G. Boucher, M. R. Boulassel, G. Ghattas, J. M. Brenchley, T. W. Schacker, B. J. Hill, D. C. Douek, J. P. Routy, E. K. Haddad, and R. P. Sekaly. 2009. HIV reservoir size and persistence are driven by T cell survival and homeostatic proliferation. *Nat. Med.* **15**:893–900.
- D'Souza-Schorey, C., B. Boettner, and L. Van Aelst. 1998. Rac regulates integrin-mediated spreading and increased adhesion of T lymphocytes. *Mol. Cell. Biol.* **18**:3936–3946.
- Ebert, L. M., P. Schaerli, and B. Moser. 2005. Chemokine-mediated control of T cell traffic in lymphoid and peripheral tissues. *Mol. Immunol.* **42**:799–809.
- Etienne-Manneville, S., and A. Hall. 2002. Rho GTPases in cell biology. *Nature* **420**:629–635.
- Eugenin, E. A., P. J. Gaskill, and J. W. Berman. 2009. Tunneling nanotubes (TNT) are induced by HIV-infection of macrophages: a potential mechanism for intercellular HIV trafficking. *Cell Immunol.* **254**:142–148.
- Fackler, O. T., and H. G. Krausslich. 2006. Interactions of human retroviruses with the host cell cytoskeleton. *Curr. Opin. Microbiol.* **9**:409–415.
- Fackler, O. T., W. Luo, M. Geyer, A. S. Alberts, and B. M. Peterlin. 1999. Activation of Vav by Nef induces cytoskeletal rearrangements and downstream effector functions. *Mol. Cell* **3**:729–739.
- Fackler, O. T., A. Moris, N. Tibroni, S. I. Giese, B. Glass, O. Schwartz, and H. G. Krausslich. 2006. Functional characterization of HIV-1 Nef mutants in the context of viral infection. *Virology* **351**:322–339.
- Feigelson, S. W., V. Grabovsky, E. Winter, L. L. Chen, R. B. Pepinsky, T. Yednock, D. Yablonski, R. Lobb, and R. Alon. 2001. The Src kinase p56(lck) up-regulates VLA-4 integrin affinity. Implications for rapid spontaneous and chemokine-triggered T cell adhesion to VCAM-1 and fibronectin. *J. Biol. Chem.* **276**:13891–13901.
- Forster, R., A. C. Davalos-Miszlitz, and A. Rot. 2008. CCR7 and its ligands: balancing immunity and tolerance. *Nat. Rev. Immunol.* **8**:362–371.
- Forster, R., A. Schubel, D. Breitfeld, E. Kremmer, I. Renner-Muller, E. Wolf, and M. Lipp. 1999. CCR7 coordinates the primary immune response by establishing functional microenvironments in secondary lymphoid organs. *Cell* **99**:23–33.
- Garcia-Bernal, D., E. Sotillo-Mallo, C. Nombela-Arrieta, R. Samaniego, Y. Fukui, J. V. Stein, and J. Teixido. 2006. DOCK2 is required for chemokine-promoted human T lymphocyte adhesion under shear stress mediated by the integrin alpha4beta1. *J. Immunol.* **177**:5215–5225.
- Green, D. S., D. M. Center, and W. W. Cruikshank. 2009. Human immunodeficiency virus type 1 gp120 reprogramming of CD4⁺ T-cell migration provides a mechanism for lymphadenopathy. *J. Virol.* **83**:5765–5772.
- Gunn, M. D., K. Tangemann, C. Tam, J. G. Cyster, S. D. Rosen, and L. T. Williams. 1998. A chemokine expressed in lymphoid high endothelial venules promotes the adhesion and chemotaxis of naive T lymphocytes. *Proc. Natl. Acad. Sci. U. S. A.* **95**:258–263.
- Haller, C., S. Rauch, N. Michel, S. Hannemann, M. J. Lehmann, O. T. Keppler, and O. T. Fackler. 2006. The HIV-1 pathogenicity factor Nef interferes with maturation of stimulatory T-lymphocyte contacts by modulation of N-Wasp activity. *J. Biol. Chem.* **281**:19618–19630.
- Hesselgesser, J., M. Liang, J. Hoxie, M. Greenberg, L. F. Brass, M. J. Orsini, D. Taub, and R. Horuk. 1998. Identification and characterization of the CXCR4 chemokine receptor in human T cell lines: ligand binding, biological activity, and HIV-1 infectivity. *J. Immunol.* **160**:877–883.
- Janardhan, A., T. Swigut, B. Hill, M. P. Myers, and J. Skowronski. 2004. HIV-1 Nef binds the DOCK2-ELMO1 complex to activate Rac and inhibit lymphocyte chemotaxis. *PLoS Biol.* **2**:e6.
- Jolly, C., K. Kashefi, M. Hollinshead, and Q. J. Sattentau. 2004. HIV-1 cell to cell transfer across an Env-induced, actin-dependent synapse. *J. Exp. Med.* **199**:283–293.
- Jolly, C., I. Mitar, and Q. J. Sattentau. 2007. Requirement for an intact T-cell actin and tubulin cytoskeleton for efficient assembly and spread of human immunodeficiency virus type 1. *J. Virol.* **81**:5547–5560.
- Lederman, M. M., and L. Margolis. 2008. The lymph node in HIV pathogenesis. *Semin. Immunol.* **20**:187–195.
- Link, A., T. K. Vogt, S. Favre, M. R. Britschgi, H. Acha-Orbea, B. Hinz, J. G. Cyster, and S. A. Luther. 2007. Fibroblastic reticular cells in lymph nodes regulate the homeostasis of naive T cells. *Nat. Immunol.* **8**:1255–1265.
- Luther, S. A., H. L. Tang, P. L. Hyman, A. G. Farr, and J. G. Cyster. 2000. Coexpression of the chemokines ELC and SLC by T zone stromal cells and deletion of the ELC gene in the plt/plt mouse. *Proc. Natl. Acad. Sci. U. S. A.* **97**:12694–12699.
- Manninen, A., M. Hiipakka, M. Vihinen, W. Lu, B. J. Mayer, and K. Saksela. 1998. SH3-domain binding function of HIV-1 Nef is required for association with a PAK-related kinase. *Virology* **250**:273–282.
- Maréchal, V., F. Clavel, J. M. Heard, and O. Schwartz. 1998. Cytosolic Gag p24 as an index of productive entry of human immunodeficiency virus type 1. *J. Virol.* **72**:2208–2212.
- Moser, B., M. Wolf, A. Walz, and P. Loetscher. 2004. Chemokines: multiple levels of leukocyte migration control. *Trends Immunol.* **25**:75–84.
- Muratori, C., L. E. Cavallin, K. Kratzel, A. Tinari, A. De Milito, S. Fais, P. D'Aloja, M. Federico, V. Vullo, A. Fomina, E. A. Mesri, F. Superti, and A. S. Baur. 2009. Massive secretion by T cells is caused by HIV Nef in infected cells and by Nef transfer to bystander cells. *Cell Host Microbe* **6**:218–230.
- Naghavi, M. H., and S. P. Goff. 2007. Retroviral proteins that interact with the host cell cytoskeleton. *Curr. Opin. Immunol.* **19**:402–407.
- Nicholson-Dykstra, S. M., and H. N. Higgs. 2008. Arp2 depletion inhibits sheet-like protrusions but not linear protrusions of fibroblasts and lymphocytes. *Cell Motil Cytoskeleton* **65**:904–922.
- Ortyn, W. E., B. E. Hall, T. C. George, K. Frost, D. A. Basiji, D. J. Perry, C. A. Zimmerman, D. Coder, and P. J. Morrissey. 2006. Sensitivity measurement and compensation in spectral imaging. *Cytometry A* **69**:852–862.
- Pabst, R., and Y. J. Rosenberg. 1998. Interpreting data on lymphocyte subsets in the blood of HIV patients—organ distribution, proliferation and migration kinetics are critical factors. *Pathobiology* **66**:117–122.
- Paluch, E., C. Sykes, J. Prost, and M. Bornens. 2006. Dynamic modes of the cortical actomyosin gel during cell locomotion and division. *Trends Cell Biol.* **16**:5–10.
- Park, I. W., and J. J. He. 2009. HIV-1 Nef-mediated inhibition of T cell migration and its molecular determinants. *J. Leukoc. Biol.* **86**:1171–1178.
- Phillips, R., and A. Ager. 2002. Activation of pertussis toxin-sensitive CXCL12 (SDF-1) receptors mediates transendothelial migration of T lymphocytes across lymph node high endothelial cells. *Eur. J. Immunol.* **32**:837–847.
- Renaud, O., J. Vina, Y. Yu, C. Machu, A. Trouve, H. Van der Voort, B. Chalmond, and S. L. Shorte. 2008. High-resolution 3-D imaging of living cells in suspension using confocal axial tomography. *Biotechnol. J.* **3**:53–62.
- Rorth, P. 2003. Communication by touch: role of cellular extensions in complex animals. *Cell* **112**:595–598.
- Rose, D. M., R. Alon, and M. H. Ginsberg. 2007. Integrin modulation and signaling in leukocyte adhesion and migration. *Immunol. Rev.* **218**:126–134.
- Rudnicka, D., J. Feldmann, F. Porrot, S. Wietgreffe, S. Guadagnini, M. C. Prevost, J. Estaquier, A. T. Haase, N. Sol-Foulon, and O. Schwartz. 2009. Simultaneous cell-to-cell transmission of human immunodeficiency virus to multiple targets through polysynapses. *J. Virol.* **83**:6234–6246.
- Rudnicka, D., and O. Schwartz. 2009. Intrusive HIV-1-infected cells. *Nat. Immunol.* **10**:933–934.
- Rustom, A., R. Saffrich, I. Markovic, P. Walther, and H. H. Gerdes. 2004. Nanotubular highways for intercellular organelle transport. *Science* **303**:1007–1010.
- Sallusto, F., D. Lenig, R. Forster, M. Lipp, and A. Lanzavecchia. 1999. Two subsets of memory T lymphocytes with distinct homing potentials and effector functions. *Nature* **401**:708–712.
- Sherer, N. M., M. J. Lehmann, L. F. Jimenez-Soto, C. Horensavitz, M. Pypaert, and W. Mothes. 2007. Retroviruses can establish filopodial bridges for efficient cell-to-cell transmission. *Nat. Cell Biol.* **9**:310–315.
- Sherer, N. M., and W. Mothes. 2008. Cytonemes and tunneling nanotubes in cell-cell communication and viral pathogenesis. *Trends Cell Biol.* **18**:414–420.
- Simon, V., and D. D. Ho. 2003. HIV-1 dynamics in vivo: implications for therapy. *Nat. Rev. Microbiol.* **1**:181–190.
- Sol-Foulon, N., C. Esnault, Y. Percherancier, F. Porrot, P. Metais-Cunha, F. Bachelier, and O. Schwartz. 2004. The effects of HIV-1 Nef on CD4 surface expression and viral infectivity in lymphoid cells are independent of raft. *J. Biol. Chem.* **279**:31398–31408.
- Sowinski, S., C. Jolly, O. Berninghausen, M. A. Purbhoo, A. Chauveau, K. Kohler, S. Oddos, P. Eissmann, F. M. Brodsky, C. Hopkins, B. Onfelt, Q. Sattentau, and D. M. Davis. 2008. Membrane nanotubes physically connect T cells over long distances presenting a novel route for HIV-1 transmission. *Nat. Cell Biol.* **10**:211–219.
- Stevenson, M. 2003. HIV-1 pathogenesis. *Nat. Med.* **9**:853–860.
- Stolp, B., M. Reichman-Fried, L. Abraham, X. Pan, S. I. Giese, S. Hannemann, P. Goulimari, E. Raz, R. Grosse, and O. T. Fackler. 2009. HIV-1 Nef

- interferes with host cell motility by deregulation of Cofilin. *Cell Host Microbe* **6**:174–186.
55. Sugimoto, C., K. Tadakuma, I. Otani, T. Moritoyo, H. Akari, F. Ono, Y. Yoshikawa, T. Sata, S. Izumo, and K. Mori. 2003. nef gene is required for robust productive infection by simian immunodeficiency virus of T-cell-rich paracortex in lymph nodes. *J. Virol.* **77**:4169–4180.
56. Takada, Y., X. Ye, and S. Simon. 2007. The integrins. *Genome Biol.* **8**:215.
57. Thoulouze, M. L., N. Sol-Foulon, F. Blanchet, A. Dautry-Varsat, O. Schwartz, and A. Alcover. 2006. Human immunodeficiency virus type-1 infection impairs the formation of the immunological synapse. *Immunity* **24**:547–561.
58. Vicente-Manzanares, M., A. Cruz-Adalia, N. B. Martin-Cofreces, J. R. Cabrero, M. Dosil, B. Alvarado-Sanchez, X. R. Bustelo, and F. Sanchez-Madrid. 2005. Control of lymphocyte shape and the chemotactic response by the GTP exchange factor Vav. *Blood* **105**:3026–3034.
59. Vicente-Manzanares, M., and F. Sanchez-Madrid. 2004. Role of the cytoskeleton during leukocyte responses. *Nat. Rev. Immunol.* **4**:110–122.
60. von Andrian, U. H., and T. R. Mempel. 2003. Homing and cellular traffic in lymph nodes. *Nat. Rev. Immunol.* **3**:867–878.
61. Xu, W., P. A. Santini, J. S. Sullivan, B. He, M. Shan, S. C. Ball, W. B. Dyer, T. J. Ketas, A. Chadburn, L. Cohen-Gould, D. M. Knowles, A. Chiu, R. W. Sanders, K. Chen, and A. Cerutti. 2009. HIV-1 evades virus-specific IgG2 and IgA responses by targeting systemic and intestinal B cells via long-range intercellular conduits. *Nat. Immunol.* **10**:1008–1017.
62. Yoder, A., D. Yu, L. Dong, S. R. Iyer, X. Xu, J. Kelly, J. Liu, W. Wang, P. J. Vorster, L. Agulto, D. A. Stephany, J. N. Cooper, J. W. Marsh, and Y. Wu. 2008. HIV envelope-CXCR4 signaling activates cofilin to overcome cortical actin restriction in resting CD4 T cells. *Cell* **134**:782–792.